ISSN 0020-4412, Instruments and Experimental Techniques, 2023, Vol. 66, No. 4, pp. 538–552. © Pleiades Publishing, Ltd., 2023.
Russian Text © The Author(s), 2023, published in Pribory i Tekhnika Eksperimenta, 2023, No. 4, pp. 21–35.

NUCLEAR EXPERIMENTAL TECHNIQUE

Studying the Operation of Silicon Photomultiplier Matrices at Cryogenic Temperatures

A. E. Bondar[a,b], E. O. Borisova[a,b,*], A. F. Buzulutskov[a,b], V. V. Nosov[a,b], V. P. Oleynikov[a,b], A. V. Sokolov[a,b], and E. A. Frolov[a,b]

[a] *Budker Institute of Nuclear Physics, Siberian Branch, Russian Academy of Sciences, Novosibirsk, 630090 Russia*

[b] *Novosibirsk State University, Novosibirsk, 630090 Russia*

**e-mail: E.O.Shemyakina@inp.nsk.su*

Received November 24, 2022; revised December 27, 2022; accepted December 29, 2022

Abstract—The performance of MPPC 13360-6050PE SiPM matrices with parallel and series connections of elements under conditions of an experiment with a two-phase detector has been investigated, and theoretical calculations of the signal characteristics have been performed for these matrices. It is shown that the signal duration does not change with a high accuracy when SiPMs are connected in series but increases with the number of SiPMs in the matrix when SiPMs are connected in parallel. Within the measurement accuracy, the integral amplitude of the signal does not depend on the number of elements in a matrix in case of the parallel connection. For the series connection, the expected decrease in the amplitude is observed, and this decrease is inversely proportional to the number of elements in the matrix. Based on the results of this study, an SiPM matrix consisting of four parallel-connected elements has been selected for further use in a two-phase cryogenic dark-matter detector since reliable detection of single-photoelectron pulses by this matrix has been demonstrated at an acceptable signal duration.

DOI: 10.1134/S002044122303003X

INTRODUCTION

Two-phase detectors based on condensed noble gases have been used to search for dark matter and detect rare events, such as coherent neutrino scattering by nuclei. In these detectors, the search for dark matter particles is carried out by observing events of their supposed elastic scattering by atomic nuclei in the liquid detector phase [1, 2]. Weakly interacting massive particles (WIMPs) now remain the leading candidates for performing the role of dark matter particles [3].

Scattering of WIMPs by nuclei of the detecting material produces recoil nuclei, which generate primary-scintillation and primary-ionization signals. The primary-scintillation signal is measured using photodetectors that view the detecting volume. Primary ionization is measured as follows: primary-ionization electrons are pulled out of the liquid into the gas phase, where they produce an electroluminescence signal under the action of an electric field, and this signal, like a primary scintillation signal, is recorded by photodetectors [2]. It is expected that scintillation and electroluminescence signals produced by a WIMP will be weak; therefore, a photodetector capable of counting single photons is required for detecting the generated light.

Photomultiplier tubes (PMTs) have been traditionally used as such detectors for detecting primary scintillations and electroluminescence in two-phase noble-gas detectors until recently. However, a global trend towards replacing PMTs with more compact silicon photomultipliers (SiPMs) has been observed today. For example, the application of SiPMs to detect scintillation and electroluminescence signals has been proposed in the DarkSide-20k project, which is a continuation of the only experiment performed worldwide with the aim of searching for dark matter using a two-phase argon detector [4, 5]. SiPMs are also considered as an alternative to PMTs in experiments on the dark-matter search based on condensed xenon [6].

Moreover, SiPMs are rapidly gaining leadership among a variety of photon detectors operable in the spectrum ranges from near UV to near IR in many fields of application [7, 8], e.g., high-energy physics [9], astrophysics [10], biology [11, 12], and medicine [13]. The range of SiPM applications is so wide because, since they belong to a new generation of photosensors, they have many advantages over traditional PMTs at a competitive price, namely, significantly lower operating voltages, a lower radioactive background level, a higher photon-detection efficiency, a compact size, and a wider spectral range [14, 15].

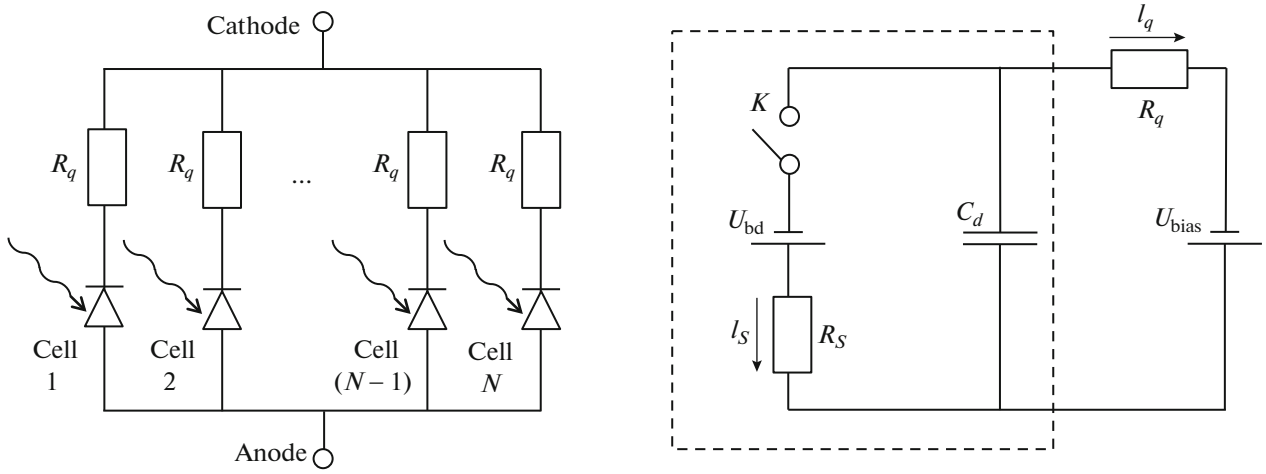

Fig. 1. Circuit diagram of the SiPM (on the left) and its individual cell (on the right).

However, SiPMs usually have a much smaller active area (on the order of 1 cm^2) in comparison with PMTs, and their use in large-scale detectors and, in particular, in dark-matter detectors leads to a sharp increase in their number. As a result, the number of electronics channels, and, hence, the number of wires must also be increased, which causes an increase in the heat flow into a cryogenic chamber.

One of the possible ways to solve the described problem is to combine several SiPMs into matrices. Several teams are now actively conducting investigations in this direction [16, 17]. However, SiPM matrices used in our two-phase cryogenic detector (MPPC S13360-6050PE, Hamamatsu, Japan) have not yet been investigated. Therefore, the important tasks are to study the operation of various configurations of MPPC S13360-6050PE SiPM matrices at a temperature of liquid argon and to select the type of a matrix with the maximum number of SiPMs at which it is still possible to work in the mode of single-photon counting. It is worth noting that this study is a continuation of the works in which we investigated the SiPM operation under cryogenic conditions [18, 19].

THEORY

Case of a Single Cell

The SiPM whose circuit diagram is shown in Fig. 1 (on the left) consists of parallel-connected cells, each of which is an avalanche photodiode operating in a Geiger mode, with a quenching resistance connected to it. Bias voltage U_{bias} is applied and the signal is read out between the cathode and the anode.

Figure 1 (on the right) shows a simplified equivalent circuit diagram of a single SiPM cell. This circuit ignores the parasitic capacitances, the input impedance of the electronics, and the influence of other cells. The avalanche photodiode is schematically outlined in Fig. 1 by a dashed line, C_d is its capacity and R_s is its resistance during breakdown. For an electron avalanche to be generated, the bias voltage must exceed the breakdown voltage U_{bd}, i.e., the minimum operating voltage at which a Geiger breakdown occurs. When a photon hits a cell, a breakdown happens, which is simulated by closure of key K that adds a source of voltage U_{bd} to the circuit [20].

Using this simplified circuit as an example, let us calculate the shape of the SiPM signal upon a breakdown using methods for calculating transients in electric circuits. Closure of the key initiates a transient process of capacitor C_d discharge, which is represented by a system of equations

$$\begin{cases} U_{\text{bd}} = I_s R_s + u_d; \\ U_{\text{bias}} = I_q R_q + u_d; \\ C_d \dot{u}_d = I_s + I_q, \end{cases} \tag{1}$$

where u_d is the voltage across capacitor C_d.

The output current I_q is the matter of interest here; therefore, by differentiating the first two equations with respect to time and by performing linear transformations, we obtain:

$$\frac{C_d \Delta U}{\tau_s \tau_q} = \frac{1}{\tau} I_q + \dot{I}_q, \tag{2}$$

where $\Delta U = U_{\text{bias}} - U_{\text{bd}}$ is the overvoltage, $\tau_{s,\,q} = R_{s,q} C_d$ are the relaxation times, and $\tau = \tau_s \tau_q / (\tau_s + \tau_q)$ is the reduced relaxation time.

Taking into account the boundary condition $R_q I_q(+0) = U_{\text{bias}} - u_d(+0) = 0$, the solution of Eq. (2) is

$$I_q(t) = \frac{C_d \Delta U}{\tau_s + \tau_q} \left(1 - e^{-\frac{t}{\tau}}\right). \tag{3}$$

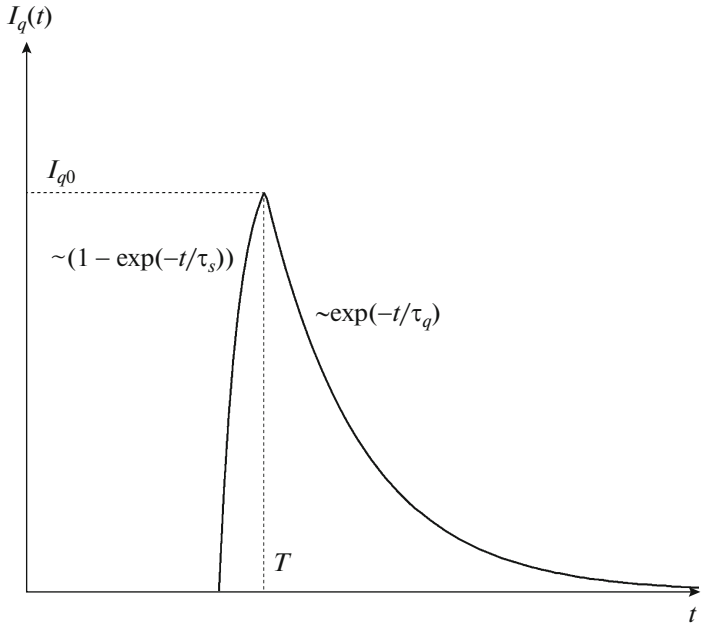

Fig. 2. Signal waveform of a single SiPM cell calculated for the ideal case.

After a certain characteristic time T, the electron avalanche fades [21], which corresponds to key opening. The subsequent process is described by a system of equations

$$\begin{cases} C_d \dot{u}_d = I_q; \\ U_{bias} = I_q R_q + u_d. \end{cases} \quad (4)$$

The solution of system (4) is

$$I_q(t) = I_{q0} e^{-(t-T)/\tau_q}, \quad (5)$$

where $I_{q0} = I_q(T) = \dfrac{C_d \Delta U}{\tau_s + \tau_q}(1 - e^{-T/\tau})$. $R_s \ll R_q$ [22]. Therefore, $\tau_s \ll \tau_q$ and $\tau \approx \tau_s$. In regard to this, the waveform described by Eqs. (3) and (5) is represented in Fig. 2. Thus, the signal has a short rise time and a long fall time. In reality, the SiPM signal waveform is different due to the influence of other cells as well as due to the presence of a parasitic capacitance between the cell and the silicon substrate. In addition, the observed waveform also depends on the response function of the electronics.

SiPM Matrices

As noted above, it was proposed that SiPMs should be combined into matrices to reduce the number of channels in the detector. Figure 3 shows the SiPM coupling for the series and parallel connections of elements. For brevity, the following designations are adopted hereafter: letters S (from series) or P (from parallel) label the type of connection, and the next symbol is the number of SiPMs connected thereby. For example, $P2$ is a matrix of two SiPMs connected in parallel, and $S3$ is a matrix of three SiPMs connected in series. A single SiPM is denoted as S (from single).

It should be noted that, when the SiPM is connected in series, a voltage applied to the matrix must be equal to the operating bias voltage of a single SiPM, multiplied by the number of elements in the matrix (N_s), since the resistance of the circuit with the series connection increases N_s times. In the case of parallel connection, the operating voltage corresponds to the voltage of a single SiPM.

The waveform of a matrix differs from the waveform of a single cell. In this case, the simplified circuit diagram (see Fig. 1, on the right) is unsuitable for calculations since it does not allow taking into account the effects of other cells, which is essential for matrices. If we modify the circuit shown in Fig. 1 (on the right) by adding the remaining cells and the input impedance of the electronics to it, the solution to the system of equations becomes much more compli-

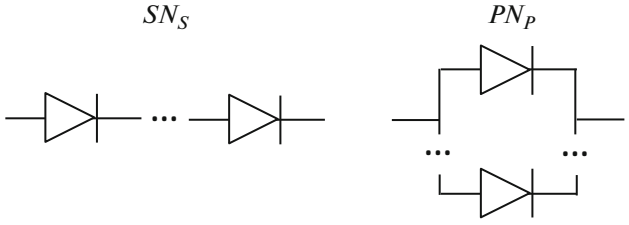

Fig. 3. Circuit diagrams of the studied types of SiPM connections: series (on the left) and parallel (on the right).

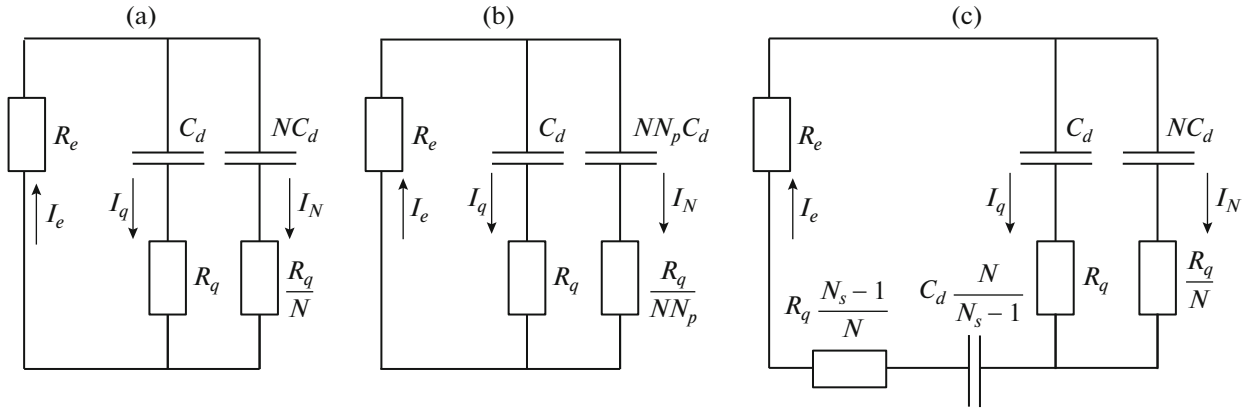

Fig. 4. Circuit diagrams of different configurations: (a) single SiPM, (b) matrix with the parallel connection of N_p SiPMs, and (c) matrix with the series connection of N_s SiPMs.

cated; therefore, we will make some simplifying assumptions. We will consider only the falling edge of the signal (i.e., the times $t \geq T$, see Fig. 2) since it is this part that makes the major contribution to the signal duration. The processes of capacitor charging or discharging occur with the same relaxation time regardless of the applied voltage; therefore, we exclude the U_{bias} source from the circuit, and the capacitance of the triggered cell will be considered charged at the initial time to a certain voltage $U(0) = U_0 \leq \Delta U$, where $\Delta U = U_{\text{bias}} - U_{\text{bd}}$.

Figure 4 shows the equivalent circuits constructed in view of the above assumptions for a single SiPM (Fig. 4a), for a matrix with the parallel connection of N_p SiPMs (Fig. 4b), and for a matrix with the series connection of N_s SiPMs (Fig. 4c). Cases $N_p = 1$ and $N_s = 1$ correspond to a single SiPM. Here, R_e is the input impedance of the electronics, R_q is the quenching resistance of a pixel, C_d is the photodiode capacitance, and N is the number of cells in the SiPM. We neglected the difference between the total number of SiPM cells (N) and the number of nontriggered cells ($N-1$), since $N \gg 1$.

The initial system of equations for the matrix with the parallel connection is

$$\begin{cases} x\dfrac{R_q}{N} I_e + R_q I_q + \dfrac{1}{C_d}\int I_q(t)\,dt = 0; \\ x\dfrac{R_q}{N} I_e + \dfrac{R_q}{NN_p} I_N + \dfrac{1}{C_d NN_p}\int I_N(t)\,dt = 0; \\ I_e = I_q + I_N, \end{cases} \qquad (6)$$

where $x = \dfrac{R_e}{R_q} N$; and I_e, I_q, and I_N are the currents through resistors R_e, R_q, and $R_q/(NN_p)$, respectively (Fig. 4b).

Since only the falling signal edge is considered, the desired current through the electronics resistor is $I_e(t) = I_0 e^{-t/\tau}$, where I_0 is the amplitude and τ is the fall time. Skipping the cumbersome calculations, we obtain the following for the parallel connection:

$$I_0 = \frac{U_0}{R_q(1 + xN_p)}, \quad \tau = \tau_q(1 + xN_p), \qquad (7)$$

where $\tau_q = R_q C_d$.

The system of equations for the matrix with the series connection has the form

$$\begin{cases} \dfrac{R_q}{N}(x + N_s - 1) I_e + \dfrac{N_s - 1}{NC_d}\int I_e(t)\,dt \\ + R_q I_q + \dfrac{1}{C_d}\int I_q(t)\,dt = 0; \\ \dfrac{R_q}{N}(x + N_s - 1) I_e + \dfrac{N_s - 1}{NC_d}\int I_e(t)\,dt \\ + \dfrac{R_q}{N} I_N + \dfrac{1}{NC_d}\int I_N(t)\,dt = 0; \\ I_e = I_q + I_N. \end{cases} \qquad (8)$$

Here, I_N is the current through the resistor R_q/N (Fig. 4c).

The solution of the system of equations in the case of the series connection is also sought in the form $I_e(t) = I_0 e^{-t/\tau}$, while the values of parameters I_0 and τ are

Table 1

Type of connection of elements in the matrix	Current amplitude I_0	Relaxation time τ	Integral amplitude A_i
Single SiPM (S)	$\propto (1+x)^{-1}$	$\propto 1+x$	const
Parallel (PN_p)	$\propto (1+xN_p)^{-1}$	$\propto 1+xN_p$	const
Series (SN_s)	$\propto (x+N_s)^{-1}$	$\propto 1+x/N_s$	$\propto 1/N_s$

$$I_0 = \frac{U_0}{R_q(x+N_s)}; \quad \tau = \tau_q\left(1+\frac{x}{N_s}\right). \tag{9}$$

Systems (6) and (8) at $N_p = 1$ and $N_s = 1$ are reduced to the case of a single SiPM, for which the values of parameters I_0 and τ are

$$I_0 = \frac{U_0}{R_q(1+x)}; \quad \tau = \tau_q(1+x). \tag{10}$$

In solutions (7), (9), and (10), there is a parameter $x = \frac{R_e}{R_q}N$, which affects the signal characteristics. The physical meaning of the parameter x is the ratio of the input impedance of the electronics R_e to the total SiPM impedance $R_{\text{tot}} = R_q/N$.

In order to estimate the value of parameter x, the impedance of the MPPC S13360-6050PE SiPM was measured using the method described in [19]. The measurement conditions were similar to the actual experimental conditions of a two-phase cryogenic detector, i.e., at an operating cryogenic temperature that is close to the boiling point of argon. A value $R_{\text{tot}} \approx 12$ kΩ was obtained. Given that the input impedance of the electronics is $R_e = 50$ Ω, we obtain $x \approx 4 \times 10^{-3} \ll 1$. The resulting value of parameter x is small compared to unity; therefore, the signal amplitude and duration of a single SiPM (see Eq. (10)) coincide with the values obtained in the case of a single cell (see Eq. (5)).

While processing the SiPM signals in experiments with the two-phase cryogenic detector, integral amplitude A_i of the SiPM photoelectron signal is calculated for further analysis. The integral amplitude of the photoelectron signal is determined as the area under the signal, $A_i = \int U(t)\,dt$, where integration is carried out over some neighborhood of the signal. Amplitude A_i is proportional to the number of detected photons (photoelectrons).

Since the major contribution to the signal is made by the trailing signal edge $I_e(t) = I_0 e^{-t/\tau}$ and its leading edge makes a much smaller contribution (see Fig. 2), the integral amplitude of the signal is represented with high accuracy by the following expression: $A_i = \int U_e(t)dt = R_e I_0 \tau$, where U_e is the voltage across resistor R_e. Let us compare the signal parameters for matrices with the parallel (7) and series (9) connections to the signal parameters of a single SiPM (10). For clarity, the results of these calculations are summarized in Table 1.

According to Table 1, we expect an increase in the signal duration and the constancy of the integral amplitude with an increase in the number of SiPMs for the parallel connection of elements in the matrix as well as a decrease in the signal duration and a decrease in the integral amplitude with an increase in the number of SiPMs for the series connection. Since $x \ll 1$ for the studied S13360-6050PE SiPMs, then, according to theoretical calculations, an increase in the number of SiPMs in the matrix is followed by a feeble change in the signal duration regardless of the connection type.

DESCRIPTION OF THE EXPERIMENTAL SETUP

We investigated Hamamatsu S13360-6050PE SiPMs [23]. They are used (Fig. 5) in the two-phase dark-matter detector being developed by Laboratory 3-3 at the Budker Institute of Nuclear Physics [24–28]. Here are their basic parameters: the active area is 6×6 mm^2, the number of pixels is 14 400, and the spectral sensitivity range is 320–900 nm [23]. At a liquid argon temperature and a bias voltage of 48 V, the noise rate is less than 0.1 Hz/mm^2, the maximum photon detection efficiency is approximately 54% at a wavelength of 460 nm [28], and the breakdown voltage at a liquid argon temperature is 42.3 ± 0.5 V.

The experimental setup was based on a cryogenic chamber cooled with liquid nitrogen (Fig. 6). The chamber was filled with argon; the thermodynamic conditions corresponded to the conditions of a real experiment: the two-phase mode was maintained inside the chamber, the temperature of the liquid argon was equal to its boiling point and is 87.3 K, and the pressure inside the chamber was 1 atm. A matrix consisting of 11 SiPMs was located in the liquid phase.

The SiPMs were powered by an A1510 module, which was a part of the CAEN SY4527 universal low-voltage power supply system. The SiPM signal was

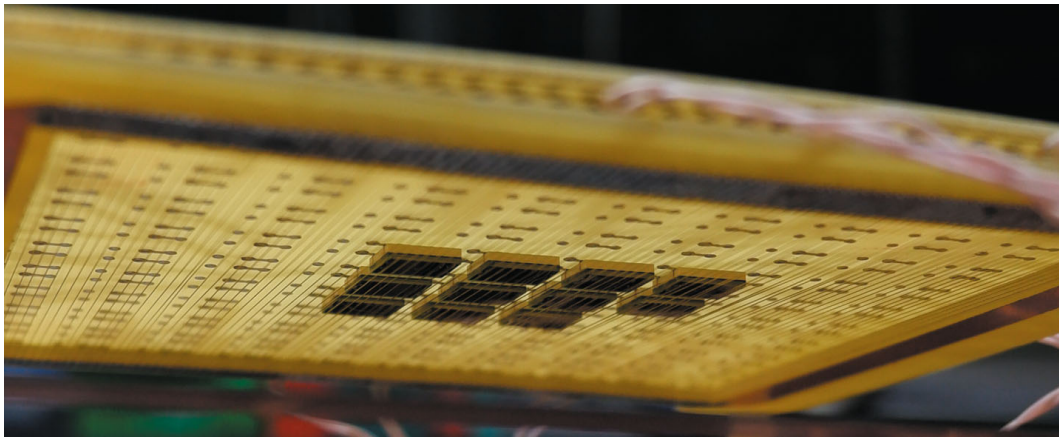

Fig. 5. Photograph of the matrix of the studied SiPMs.

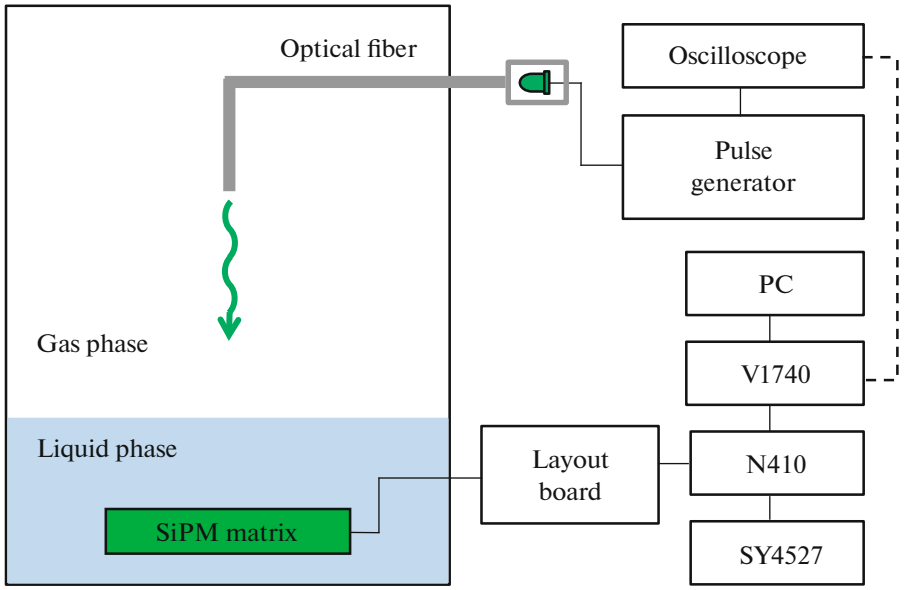

Fig. 6. Layout of the experimental setup. The trigger-signal transfer line is shown with a dashed line.

amplified using the NAICAM N410 amplifier with a shaping time of 40 ns and a gain of 56. Between the amplifier and the SiPM, there was a layout board that allowed SiPM switching. The amplified SiPM signals were digitized using the CAEN V1740 analog-to-digital converter (ADC) and transmitted to a computer for visualization and recording.

The intrinsic noise of the studied SiPMs was practically absent at the liquid-argon temperature. The amplitude spectra were measured when the SiPM matrix was illuminated by an LED emitting at a wavelength of 565 nm. An optical fiber was laid inside the chamber, while the LED itself was located outside the chamber; this allowed minimizing the noise pickup level of the SiPMs.

Rectangular voltage pulses with a duration of 60 μs was supplied from a pulse generator for the LED. The pulse amplitude was selected so that the number of photons detected by the SiPMs was small enough to avoid strong distortions of the signal baseline and pileup of single-photon pulses. The generator signal was split and also fed to the oscilloscope, which produced a trigger signal for the ADC.

The measurements were performed in the bias-voltages range of 44–50 V with a step of 1 V. The upper limit was determined by the initiation of a self–sustaining SiPM breakdown, and the lower limit was determined by the ability to detect single-photoelectron peaks against the background of external stray pickup. A bias voltage of 46 V is the most interesting for us since it is the optimal operating voltage for the two-phase dark-matter detector used in our labora-

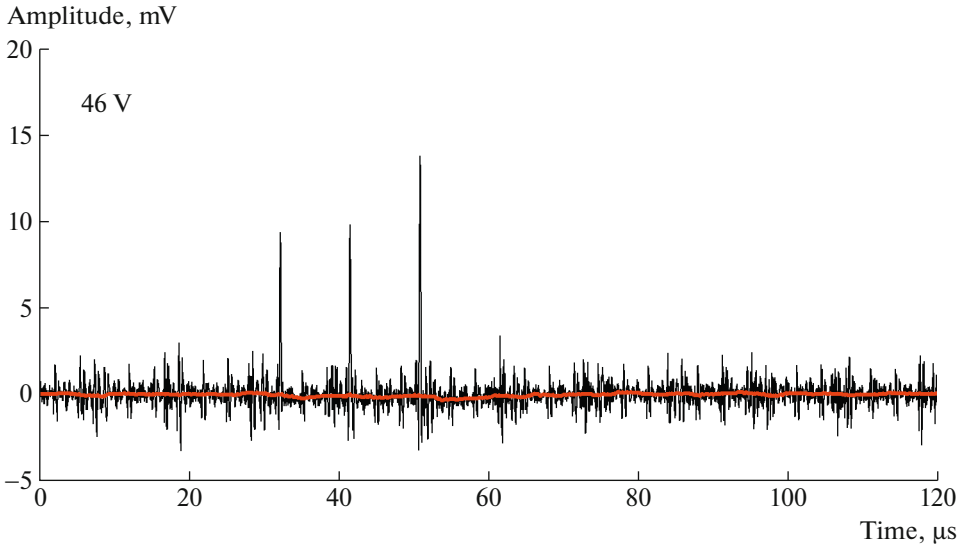

Fig. 7. Ray trace of the SiPM signal at a bias voltage of 46 V. The thick red line shows the baseline obtained using the median filter that was used in the signal processing to account for the baseline offset associated with the operation of amplifiers.

tory: the gain attained at this voltage is sufficient for reliable detection of single-photon signals, and the probability of optical crosstalk is not too high yet.

The signal was recorded by a personal computer (PC) in the form of events with a duration of 160 μs. Figure 7 shows an example of the SiPM signal waveform at a bias voltage of 46 V. Photoelectron peaks caused by detection of photons are observed in the time interval of 15–75 μs where the LED was in the emitting state. These peaks are quite rare; therefore, the probability that peaks overlap is not so high. The thick red line in Fig. 7 shows the baseline obtained using the median filter. This filter was used in the signal processing to account for the baseline offset associated with the operation of the amplifiers.

RESULTS AND DISCUSSION

Signal Waveform

When studying the signal waveform, we selected peaks whose amplitude was higher than the noise pickup level and lower than a certain threshold corresponding to the boundary between the single- and two-photoelectron signals. The centers of the selected peaks were superposed, after which averaging was carried out over a sample of 1000 peaks.

Figure 8 shows the waveforms averaged over events and normalized to the amplitude of a single SiPM, at a bias voltage of 46 V for matrices with parallel ($P2 - P9$, Fig. 8a) and series ($S2$ and $S3$, Fig. 8b) connections of elements. The waveform of a single SiPM (S) is shown for comparison. The maximum points of the curves are superposed. It can be seen that, as the number of SiPMs increases, the signal duration remains constant for the series connection, as expected. However, the signal duration increases for the parallel connection. Most likely, this is caused by the operation of the amplifier: when SiPMs in the matrix with the parallel connection increase in number, the total capacitance at the input of the charge-sensitive amplifier increases. This increases the signal distortion by the amplifier since the presented signal waveforms are determined not only by the type of connection of the elements but also by the response function of the amplifiers. Table 2 presents the absolute values of the full width at half-maximum (FWHM) of the signals as well as the relative increase (Δ) of this value compared to a single SiPM for matrices with the parallel connection of their elements ($P2 - P9$).

Amplitude Spectra

When the amplitude characteristics were investigated, the integral amplitude was calculated for each peak that exceeded a preset threshold. This threshold was selected so that all single-photoelectron peaks were detected. The integral amplitude of a peak was calculated as its area in the part where the signal exceeded the baseline reconstructed using the median

Table 2. Signal duration characteristics for matrices with the parallel SiPM connection: full width at half-maximum (FWHM) as well as the relative increase (Δ) of this value compared to a single SiPM

Characteristics	SiPM matrix configuration								
	S	$P2$	$P3$	$P4$	$P5$	$P6$	$P7$	$P8$	$P9$
FWHM, ns	226	237	255	270	293	308	327	337	350
Δ, %	0	5	13	19	30	36	45	49	55

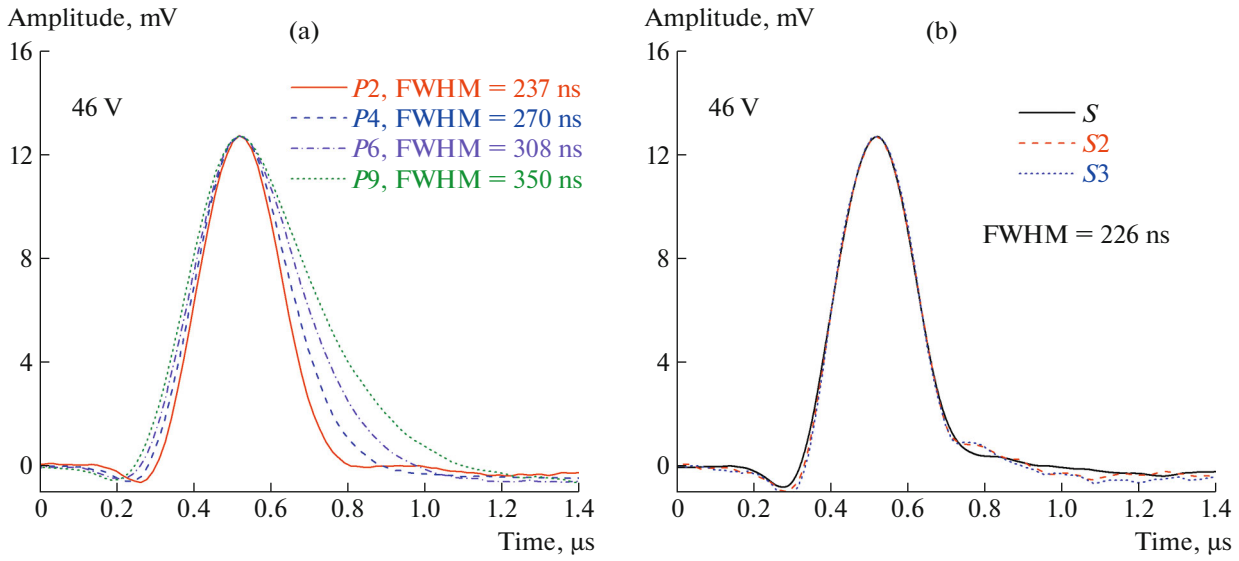

Fig. 8. Waveforms, averaged over events and normalized to the amplitude of a single SiPM, at a bias voltage of 46 V for matrices with (a) parallel ($P2 - P9$) and (b) series ($S2$ and $S3$) connections of SiPMs; the waveform of a single SiPM (S) is shown for comparison.

filter. A histogram of the calculated amplitudes was then plotted.

Figure 9 shows the amplitude spectra obtained thereby for a single SiPM (for the first channel) at various bias voltages. The left peak corresponds to the external noise pickup; it appeared because some of the signals associated with the external noise pickup exceed the specified threshold, but the area of such signals is small. The next, well-separable central peak corresponds to the single-photon detection by a SiPM. A peak corresponding to the two-photoelectron signal is also clearly discernible at low bias voltages (up to 47 V), and the presence of this signal is associated, in particular, with optical crosstalk of SiPMs [29]. As the bias voltage grows in value, the integral amplitudes increase and the peaks become more and more asymmetric, which is associated with an increase in the probability of afterpulses [29]. Incidentally, the second peak becomes hardly distinguishable.

The amplitude spectra of matrices with the parallel connection of different numbers of SiPMs ($P2 - P5$) at a bias voltage of 46 V are shown in Fig. 10. According to Fig. 10, the mean integral amplitude of a single-photoelectron signal (A_{1pe}) for matrices with the parallel connection of elements is comparable to the amplitude of a single SiPM. In addition, an increase in the number of SiPMs in the matrix leads to spectrum broadening and blurring, because an increase in the number of SiPMs in the matrix with the parallel connection is followed by an increase in the input capacitance of the charge-sensitive amplifier, which, in turn, raises the noise level [30].

Figure 11 shows the amplitude spectra of a matrix with two serially connected SiPMs ($S2$). The spectrum obtained at a SiPM voltage of 46 V is shown on the left. It can be seen that the peak due to the external noise pickup and the spectrum of SiPM signals merge, which makes it difficult to identify each part of the spectrum. The spectrum obtained at a SiPM voltage of 48 V is shown on the right; here, the peak of the external noise pickup is separable from the signal spectrum. This allows us not only to estimate the amplitude of a single-photoelectron SiPM signal at a voltage of 48 V but also to understand the relative position of the noise peak and the signal spectrum at lower SiPM voltages and at 46 V in particular. It can be seen that the mean integral amplitude of the single-photoelectron signal from the $S2$ matrix is much lower relative to a single SiPM (Fig. 9) at equal bias voltages. The spectrum itself looks more blurred, and the peak corresponding to the detection of two photoelectrons is hardly visible. The latter can be attributed, in particular, to the fact that, when signals are rare, the current passing through a chain of SiPMs connected in series appears to be low, which leads to nonuniform distribution of the voltage between the SiPMs.

Amplitude Characteristics

It is a common practice to use the dependence of the mean integral amplitude of a single-photoelectron signal on the bias voltage to describe the SiPM performance since it allows one, after appropriate calibration, to determine the amplification characteristic of the SiPM, which is represented by a linear function [23]. The mean integral amplitude of a single-photo-

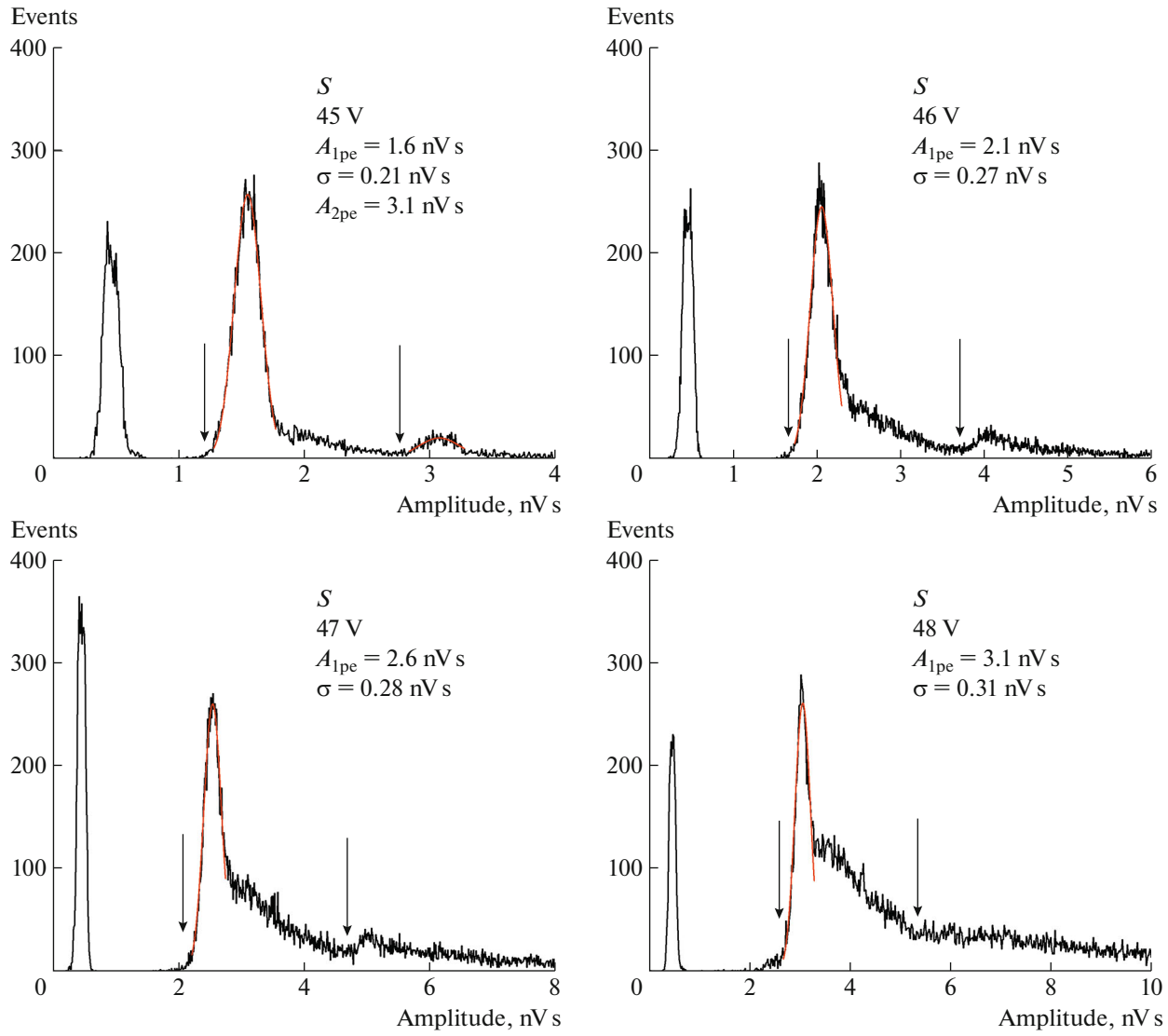

Fig. 9. Amplitude spectra of a single SiPM at different bias voltages.

electron signal is determined in this case as the difference in the mean amplitude of adjacent peaks in the amplitude distribution or as the position of the first peak relative to zero. It should be noted that this method is applicable when the peaks of the distribution are symmetric, as was the case, e.g., in [31]. However, as can be seen from Figs. 9–11, the presence of a right tail in photoelectron peaks associated with afterpulses is a feature of the tested SiPM. In such a situation, the problem of a method for determining the mean integral amplitude of a single-photoelectron signal becomes relevant.

We see two possible methods. In the first one, we propose estimation of the mean amplitude by that part of the spectrum that includes the tail on the right (in Fig. 9, these areas are highlighted with arrows). In the second method, we propose to use of only the symmetric part of the peak, discarding the tail, to fit this part with the Gaussian function (see the fits in Figs. 9–11), and obtain thereby the estimates for the mean value and rms deviation.

Figure 12 shows the dependences of the mean amplitude of the single-photoelectron signal for single SiPMs, which were obtained using the described methods. The data were averaged over 11 available channels. The maximum deviation from the mean was taken as the errors. The solid circles show the data obtained using the symmetrical part of the peak, and the solid line shows the linear approximation of these points. The light squares show the data obtained in view of the right tail, while the dashed line is the linear approximation drawn through the first three points.

According to Fig. 12, the higher the bias voltage, the greater is the difference between the amplitudes determined using different methods. This fact can be

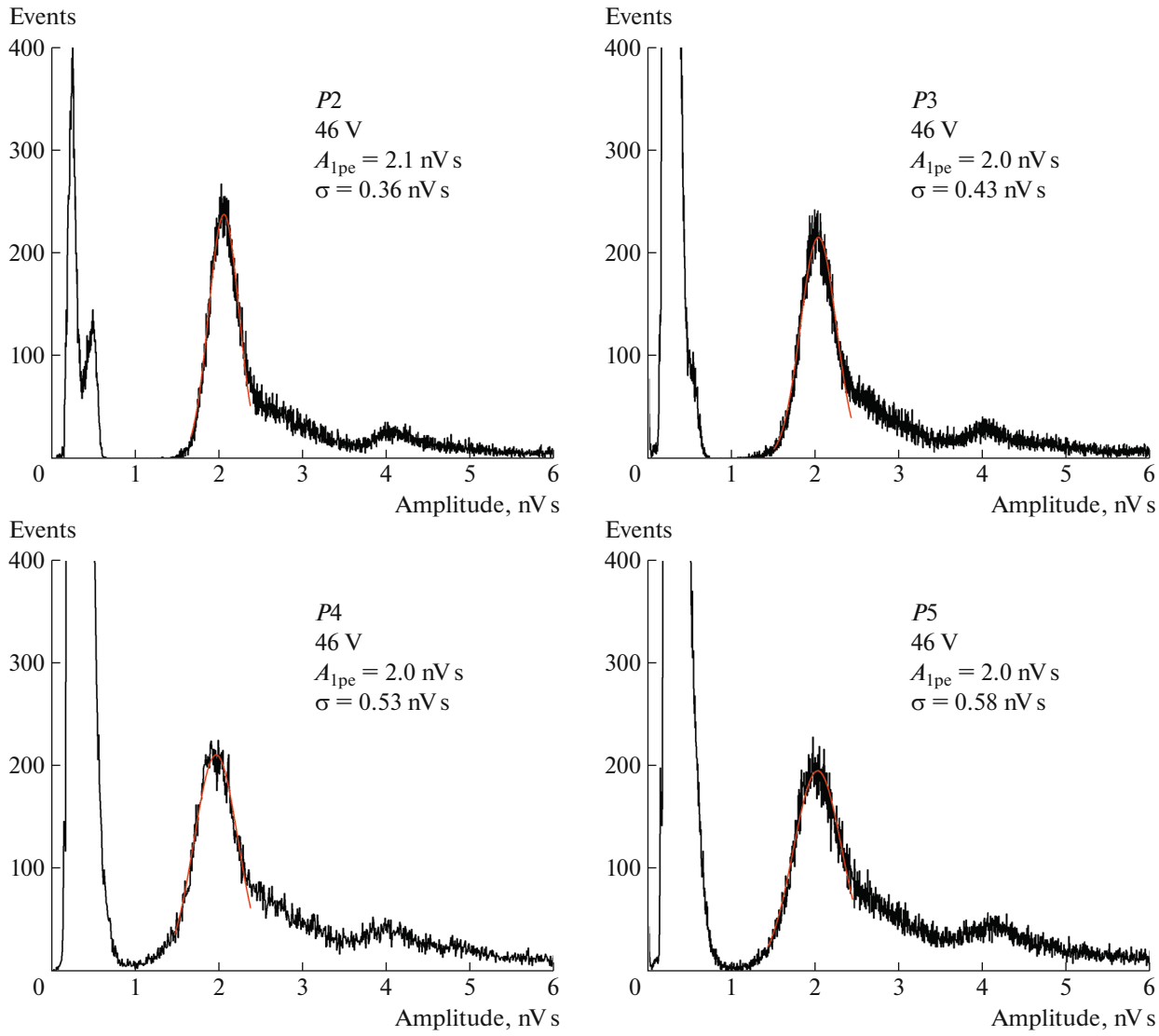

Fig. 10. Amplitude spectra of matrices with the parallel connection of different numbers of SiPMs ($P2 - P5$) at a bias voltage of 46 V.

attributed to the increase in the probability of afterpulses with an increase in the bias voltage. Unlike the data obtained with account for the right tail, the points obtained using the symmetric part of the peak are represented by the linear dependence (as expected) owing to the linearity of the amplification characteristic. Therefore, from now on, we calculate the amplitude dependences using the method in which only the symmetric part of the peak is taken into account.

Figure 13 shows the voltage dependences of the mean amplitude of a single-photoelectron signal for matrices with parallel-connected ($P2 - P5$) and series-connected elements ($S2$). The dependences are represented by linear functions within the measurement accuracy. In addition, the data for the $P2 - P5$ matrices coincide within the measurement accuracy. As expected, the amplitude of a single-photoelectron signal for the $S2$ matrix is less than the amplitude for a single SiPM and, within the measurement accuracy, the dependence of the amplitude on the number of SiPMs in the matrix is $A_i^{SN_s}/A_i^S = 1/N_s$. Table 3 presents the linear parameterization coefficients $A_i = (V - U_{bd})G$, which describe the voltage dependence of the mean amplitude of the single-photoelectron signal for different matrices.

Noise Pickup Level

In addition to the parameters of photoelectron signals, the levels of external noise pickup were investigated for various SiPM matrices. For this purpose, for each channel, the rms deviation from the mean value was calculated among the set of y coordinates of each point in the time range where events do not contain

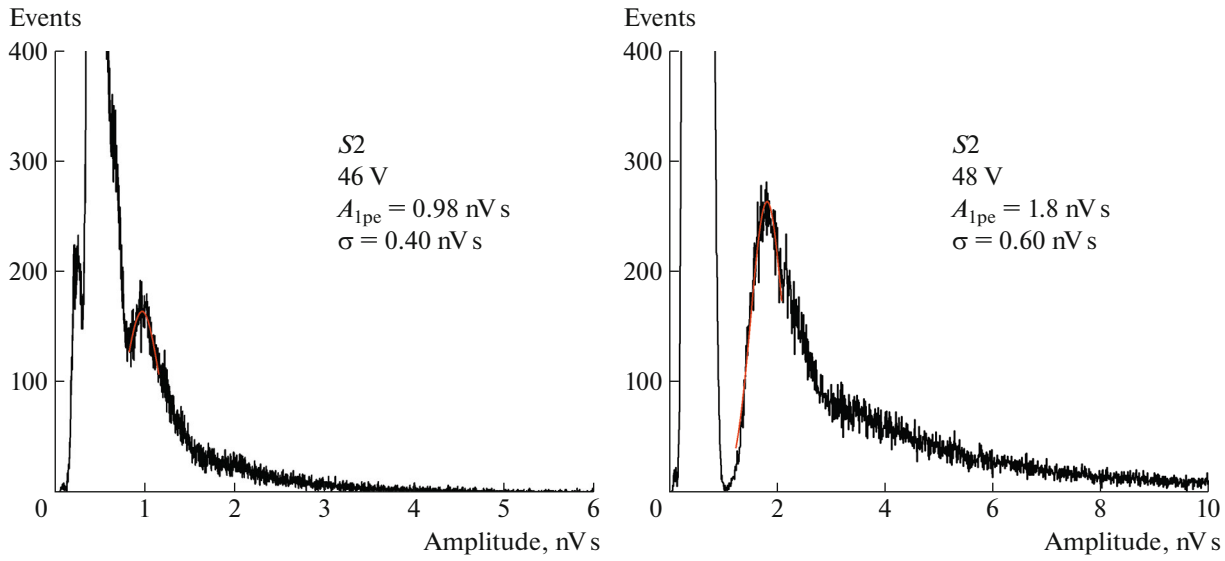

Fig. 11. Amplitude spectra of the matrix with the series connection (*S*2) at bias voltages of 46 V (on the left) and 48 V (on the right).

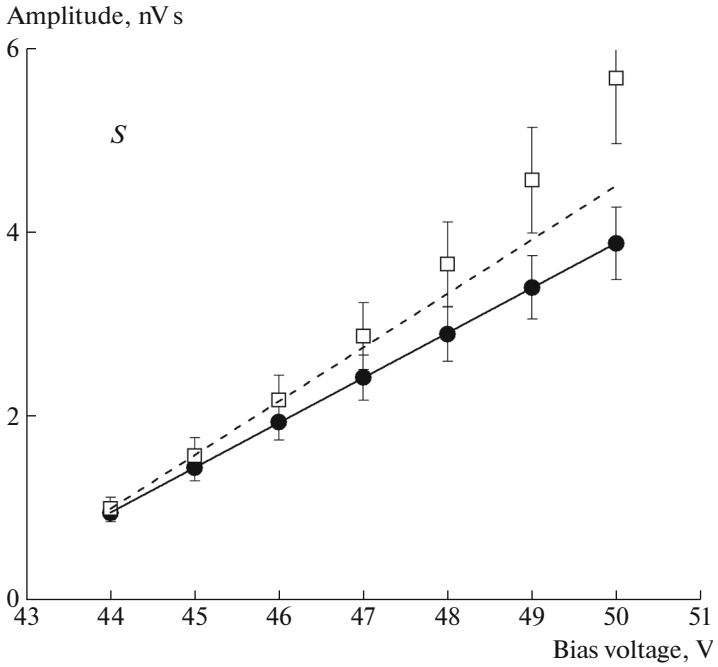

Fig. 12. Voltage dependence of the mean amplitude of a single-photoelectron signal, calculated as the average over the part of the spectrum including the tail (open squares) and as the average over the symmetrical part of the spectrum (solid circles), for a single SiPM. The data were averaged over 11 available channels.

photoelectron peaks (90–160 μs; see Fig. 7). The obtained values were averaged initially over all channels (for all matrices except *P*6–*P*9, in which there was only one channel), and then over a sample of 1000 events; the rms deviation of the values in this sample was taken as an uncertainty.

Figure 14 shows the dependence of the noise pickup level on the number of SiPMs in the matrix at a bias voltage of 46 V. It can be seen that the noise pickup level initially increases with an increase in the number of SiPMs in the matrix and reaches a plateau when more than six SiPMs are connected.

Discussion of the Results

The results obtained by the other teams, at first glance, somewhat contradict our results [16, 17, 32, 33]. In particular, it was stated that, when SiPMs are

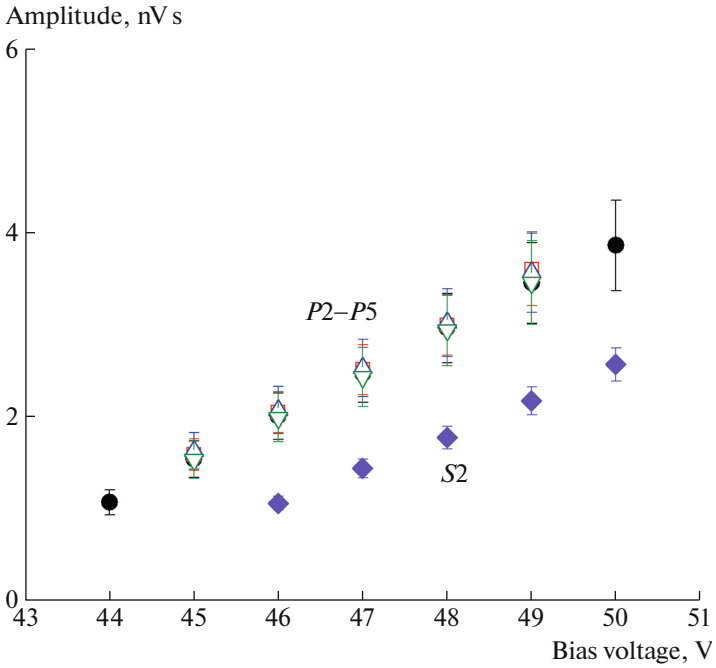

Fig. 13. Dependence of the mean amplitude of a single-photoelectron signal on the voltage for matrices with the parallel connection of different numbers of SiPMs ($P2 - P5$) and with the series connection of SiPMs ($S2$).

connected in series, the signal from the matrix turns out to be faster than the signal from a single SiPM [32]. Apparently, this is explained by the fact that parameter x was not small in those works, unlike our work. In our case, the measurements were carried out at a cryogenic temperature when the quenching resistance increased by 10–100 times [19] compared to room temperature, which leads to a decrease in the x parameter.

Let us take a closer look at the advantages and disadvantages of the studied types of connections. Automatic overvoltage control is considered to be an advantage of the series connection [32]. It eliminates the need to select SiPMs with equal breakdown voltages, which is especially important in experiments where the number of SiPM channels is large. On the other hand, when signals are rare (in particular, at cryogenic temperatures, when the SiPM noise rate is low), the current passing through a chain of series-connected SiPMs turns out to be low, which prevents automatic overvoltage adjustment. The other advantage of the series connection is a faster signal compared to the parallel connection [32]. At the same time, the series connection also has drawbacks, in particular: the need for a higher bias voltage (proportional to the number of SiPMs in the matrix) and the lower amplitude compared to single SiPMs.

Table 3. Coefficients of linear functions representing the dependences of the mean amplitude of a single-photoelectron signal on the voltage for various matrices

Parameterization constant	SiPM configuration					
	S	$P2$	$P3$	$P4$	$P5$	$S2$
G, ns	0.49	0.47	0.49	0.48	0.47	0.37
U_{bd}, V	42.1	41.7	41.8	41.6	41.8	43.1

An advantage of the parallel connection is as follows: for matrices with this type of connection, the signal amplitude does not change with an increase in the number of SiPMs, and the bias voltage for a matrix remains the same as for a single SiPM. However, the signal duration from a matrix with parallel-connected SiPMs increases, albeit slightly, but this is a disadvantage for fast measurements. In addition, SiPMs with similar breakdown voltages must be selected for the parallel connection [33] in order to obtain similar performance characteristics of each SiPM in the matrix, in particular, close single-photoelectron amplitudes and probabilities of optical crosstalk. Since the MPPC S13360-6050PE SiPMs we used feature a small variation in the breakdown voltage, individual selection of SiPMs was not required in our study.

CONCLUSIONS AND SUMMARY

In this work, we studied the performance of MPPC S13360-6050PE SiPM matrices with the parallel and series connection of elements at the temperature of liquid argon for use in a two-phase cryogenic dark-

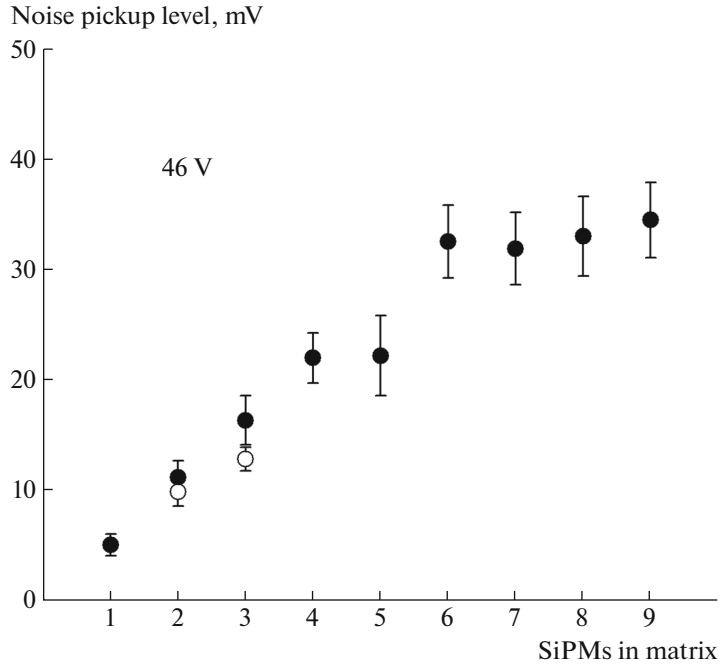

Fig. 14. Dependence of the noise pickup level (rms deviation) on the number of SiPMs in a matrix at a bias voltage of 46 V: single SiPM and matrices with the parallel connection of different numbers of SiPMs ($P2 - P9$) are shown with solid circles, and matrices with the series SiPM connection ($S2$ and $S3$) are shown with open circles.

matter detector being developed by the Budker Institute of Nuclear Physics.

The theoretical calculations of the signal characteristics (the amplitude and duration) were carried out for a single SiPM and for matrices with parallel and series connections of elements. The results of these calculations include parameter $x = \frac{R_e}{R_q} N$, which determines the nature of the signal change when SiPMs are combined into matrices. The total quenching resistance $R_{\text{tot}} = R_q/N$ of SiPMs at cryogenic temperature was measured to estimate the value of this parameter. It turned out that $x \approx 4 \times 10^{-3} \ll 1$. At such a small parameter, it is expected that the signal duration at the series and parallel connections will coincide with the duration of the signal from a single SiPM with a high accuracy. It is also expected that the integral amplitude will remain constant with an increase in the number of elements in the parallel connection and decrease inversely proportional to the number of elements in the series connection.

The SiPM matrices with the parallel ($P2 - P9$) and series ($S2$,$S3$) connections of elements have been experimentally studied. The signal duration from the series-connected SiPMs did not change with a high accuracy, which is consistent with the theory. The duration of the signal from the matrix with the parallel connection increases with the number of SiPMs in the matrix, which contradicts the performed estimates. Most likely, this can be attributed to the operation of the amplifier: an increase in the number of SiPMs in the matrix with the parallel connection of elements is followed by an increase in the total capacitance at the input of the charge-sensitive amplifier, which results in a stronger signal distortion by the amplifier.

The experiment confirmed that the number of elements in the matrix with the parallel connection does not affect the integral signal amplitude within the measurement accuracy. At the same time, an expected decrease in the integral amplitude is observed in matrices with the series connection, and this decrease is inversely proportional to the number of elements in the matrix within the measurement accuracy.

The noise pickup level initially increases with an increase in the number of SiPMs in the matrix, and this is true for any type of connection of elements. Upon further increase in the number of SiPMs, the dependence reaches a plateau. For matrices with the series connection, the noise pickup level occurs comparable to the signal, which makes it difficult to determine the amplitude of a single-photoelectron signal from the spectrum. The same applies to matrices with the parallel connection of more than five elements.

Thus, according to the results of this study, an SiPM matrix consisting of four parallel-connected elements ($P4$) has been selected for further use in a two-phase cryogenic detector of dark matter since reliable measurement of single-photoelectron pulses against an external background has been demonstrated

for this matrix type, and the signal duration has moderately (by 20%) increased compared to a single SiPM. In addition, it is convenient to arrange the four elements in the form of a square, obtaining photosensors with dimensions of 1.2 × 1.2 cm.

FUNDING

This work was supported in part by the Russian Science Foundation (project no. 21-72-00014).

CONFLICT OF INTEREST

The authors declare that they have no conflicts of interest.

REFERENCES

1. Akimov, D.Y., Bolozdynya, A.I., Buzulutskov, A.F., and Chepel, V., *Two-Phase Emission Detectors,* World Scientific, 2021, p. 1.332. https://doi.org/10.1142/12126
2. Chepel, V. and Araujo, H., *J. Instrum.,* 2013, vol. 8, p. R04001. https://doi.org/10.1088/1748-0221/8/04/R04001
3. Arcadi, G., Dutra, M., Ghosh, P., Lindner, M., Mambrini, M., Pierre, M., Profumo, S., and Queiroz, F. S., *Eur. Phys. J. C,* 2018, vol. 78, p. 203. https://doi.org/10.1140/epjc/s10052-018-5662-y
4. DarkSide Collab., Aalseth, C.E., et al., *Eur. Phys. J. Plus,* 2018, vol. 133, p. 129. https://doi.org/10.1140/epjp/i2018-11973-4
5. DarkSide Collab., Aalseth, C.E., et al., *Eur. Phys. J. C,* 2021, vol. 81, p. 163. https://doi.org/10.1140/epjc/s10052-020-08801-2
6. Baudis, L., Galloway, M., Kish, A., Marentini, C., and Wulf, J., *J. Instrum.,* 2018, vol. 13, p. 10022. https://doi.org/10.1088/1748-0221/13/10/P10022
7. Acerbi, F., Paternoster, G., Capasso, M., Marcante, M., Mazzi, A., Regazzoni, V., Zorzi, N., and Gola, A., *Instruments,* 2019, vol. 3, p. 15. https://doi.org/10.3390/instruments3010015
8. Yamamoto, K., Nagano, T., Yamada, R., Ito, T., and Ohashi, Y., *JPS Conf. Proc.,* 2019, vol. 27, p. 011001. https://doi.org/10.7566/JPSCP.27.011001.
9. Garutti, E., *J. Instrum.,* 2011, vol. 6, p. C10003. https://doi.org/10.1088/1748-0221/6/10/C10003
10. Anderhub, H., Backes, M., Biland, A., Boccone, V., Braun, I., Bretz, T., Bu, J., Cadoux, F., Commichau, V., Djambazov, L., Dorner, D., Einecke, S., Eisenacher, D., Gendotti, A., Grimm, O., et al., *J. Instrum.,* 2013, vol. 8, p. P06008. https://doi.org/10.1088/1748-0221/8/06/P06008
11. Mora, A.D., Martinenghi, E., Contini, D., Tosi, A., Boso, G., Durduran, T., Arridge, S., Martelli, F., Farina, A., Torricelli, A., and Pifferi, A., *Opt. Express,* 2015, vol. 23, no. 11, p. 13937. https://doi.org/10.1364/OE.23.013937
12. Modi, M.N., Daie, K., Turner, G.C., and Podgorski, K., *Opt. Express,* 2019, vol. 27, no. 24, p. 35830. https://doi.org/10.1364/OE.27.035830
13. Otte, A.N., Barral, J., Dolgoshein, B., Hose, J., Klemin, S., Lorenz, E., Mirzoyan, R., Popova, E., and Teshima, M., *Nucl. Instrum. Methods Phys. Res., Sect. A,* 2005, vol. 545, no. 3, p. 705. https://doi.org/10.1016/j.nima.2005.02.014
14. Renker, D., *Nucl. Instrum. Methods Phys. Res., Sect. A,* 2006, vol. 567, p. 48. https://doi.org/10.1016/j.nima.2006.05.060
15. Ozaki, K., Kazama, S., Yamashita, M., Itow, Y., and Moriyama, S., *J. Instrum.,* 2021, vol. 16, p. P03014. https://doi.org/10.1088/1748-0221/16/03/P03014
16. Cervi, T., Babicz, M.E., Bonesini, M., Falcone, A., Kose, U., Nessi, M., Menegolli, A., Pietropaolo, F., Raselli, G.L., Rossella, M., Torti, M., and Zani, A., *J. Instrum.,* 2017, vol. 12, p. C03007. https://doi.org/10.1088/1748-0221/12/03/C03007
17. D'Incecco, M., Galbiati, C., Giovanetti, G.K., Korga, G., Li, X., Mandarano, A., Razeto, A., Sablone, D., and Savarese, C., *IEEE Trans. Nucl. Sci.,* 2017, vol. 65, p. 591. https://doi.org/10.1109/TNS.2017.2774779
18. Bondar, A., Buzulutskov, A., Dolgov, A., Shemyakina, E., and Sokolov, A., *J. Instrum.,* 2015, vol. 10, p. P04013. https://doi.org/10.1088/1748-0221/10/04/P04013
19. Bondar, A., Buzulutskov, A., Dolgov, A., Shekhtman, L., Shemyakina, E., Sokolov, A., Breskin, A., and Thers, D., *J. Instrum.,* 2014, vol. 9, p. P08006. https://doi.org/10.1088/1748-0221/9/08/P08006
20. Popova, E.V., Buzhan, P.Zh., Stifutkin, A.A., Ilyin, A.L., Mavritskii, O.B., Egorov, A.N., and Nastulyavichius, A.A., *J. Phys.: Conf. Ser.,* 2016, vol. 737, p. 012041. https://doi.org/10.1088/1742-6596/737/1/012041
21. Cova, S., Ghioni, M., Lacaita, A., Samori, C., and Zappa, F., *Appl. Opt.,* 1996, vol. 35, no. 12, p. 1956. https://doi.org/10.1364/AO.35.001956
22. https://hub.hamamatsu.com/us/en/technical-notes/mppc-sipms/what-is-an-SiPM-andhow-does-it-work.html.
23. https://www.hamamatsu.com/.
24. Bondar, A., Buzulutskov, A., Grebenuk, A., Pavluchenko, D., Snopkov, R., Tikhonov, Y., Kudryavtsev, V.A., Lightfoot, P.K., and Spooner, N.J.C., *Nucl. Instrum. Methods Phys. Res., Sect. A,* 2007, vol. 574, p. 493. https://doi.org/10.1016/j.nima.2007.01.090
25. Bondar, A., Buzulutskov, A., Dolgov, A., Nosov, V., Shekhtman, L., Shemyakina, E., and Sokolov, A., *Europhys. Lett.,* 2015, vol. 112, p. 19001. https://doi.org/10.1209/0295-5075/112/19001
26. Bondar, A., Borisova, E., Buzulutskov, A., Frolov, E., and Sokolov, A., *J. Instrum.,* 2020, vol. 15, p. C06064. https://doi.org/10.1088/1748-0221/15/06/C06064
27. Buzulutskov, A., Frolov, E., Borisova, E., Nosov, V., Oleynikov, V., and Sokolov, A., *Eur. Phys. J. C,* 2022, vol. 82, p. 839. https://doi.org/10.1140/epjc/s10052-022-10792-1
28. Aalseth, C.E., Abdelhakim, S., Agnes, P., Ajaj, R., Albuquerque, I.F.M., Alexander, T., Alici, A., Alton, A.K., Amaudruz, P., Ameli, F., Anstey, J., Antonioli, P., Arba, M., Arcelli, S., Ardito, R., et al., *Eur. Phys. J. C,* 2021, vol. 81, p. 153. https://doi.org/10.1140/epjc/s10052-020-08801-2

29. Rosado, J. and Hidalgo, S., *J. Instrum.,* 2015, vol. 10, p. P10031. https://doi.org/10.1088/1748-0221/10/10/P10031

30. Horowitz, P. and Hill, W., *The Art of Electronics,* Cambridge Univ. Press, 2015, chap. 8.5.7, pp. 497–499, chap. 8.11.3, pp. 538–539.

31. Bondar, A., Buzulutskov, A., Grebenuk, A., Sokolov, A., Akimov, D., Alexandrov, I. and Breskin, A., *J. Instrum.,* 2010, vol. 5, p. P08002. https://doi.org/10.1088/17480221/5/08/p08002

32. Collazuol, G., *Proc. 15th Vienna Conference on Instrumentation VCI-2019,* Vienna: Vienna Univ. of Technology, February 18–22, 2019, p. 86. https://indi.to/DyMp5.

33. Cervi, T., Babicz, M., Bonesini, M., Falcone, A., Menegolli, A., Raselli, G.L., Rossella, M., and Torti, M., *Nucl. Instrum. Methods Phys. Res., Sect. A,* 2018, vol. 912, p. 209. https://doi.org/10.1016/j.nima.2017.11.038

Translated by N. Goryacheva